AIAA-2000-1586

GROUND VIBRATION TEST PLANNING AND PRE-TEST ANALYSIS FOR THE X-33 VEHICLE

Herand Bedrossian *
Lockheed Martin Skunk Works
1011 Lockheed Way
Palmdale, CA 93599-2545

Michael L. Tinker ** and Homero Hidalgo †
Structural Dynamics and Loads Group/ED21
Structures, Mechanics, and Thermal Department
NASA/Marshall Space Flight Center
Huntsville, AL 35812

Abstract

This paper describes the results of the modal test planning and the pre-test analysis for the X-33 vehicle. The pre-test analysis included the selection of the target modes, selection of the sensor and shaker locations and the development of an accurate Test Analysis Model (TAM). For target mode selection, four techniques were considered; one based on the Modal Cost technique, one based on Balanced Singular Value technique, a technique known as the Root Sum Squared (RSS) method, and a Modal Kinetic Energy (MKE) approach. For selecting sensor locations, four techniques were also considered; one based on the Weighted Average Kinetic Energy (WAKE), one based on Guyan Reduction (GR), one emphasizing engineering judgment, and one based on a Genetic Algorithm (GA) technique. For selecting shaker locations, four techniques were also considered; one based on the Weighted Average Driving Point Residue (WADPR), one based on engineering judgment and accessibility considerations, a frequency response method, and a GA- based technique.

To evaluate the effectiveness of the proposed sensor and shaker locations, two well-known frequency response function (FRF) based numerical simulation techniques were used. The two techniques included the Multivariate Mode Indicator Function (MMIF) and, the Complex Mode Indicator Function (CMIF). Both techniques showed the effectiveness of the sensor and shaker set with respect to modal parameter identification. Several TAM reduction techniques were considered including Guyan, IRS, Modal, and Hybrid. A Hybrid TAM reduction technique was used for three vehicle fuel level configurations.

* Research & Development Engineer, Senior Member AIAA, Member ASME

**Aerospace Technologist, Structural Dynamics; Senior Member AIAA

†Aerospace Technologist, Structural Dynamics

Introduction

The X-33 is an advanced technology demonstrator vehicle for the Reusable Launch Vehicle (RLV) program (Fig. 1). Due to cost and schedule issues, the real X-33 flight vehicle will be used during the vehicle Ground Vibration Test (GVT) or modal survey test. The X-33 vehicle will be mounted on a soft airbag isolation system and positioned vertically to simulate the free flight condition, as shown in Fig. 2. Objectives of the GVT include the following:

1. Measure vehicle primary modes, frequencies, and damping for three flight configurations: empty, partially-fueled, and fully-fueled; required for control and liftoff loads.
2. Identify modes of aerodynamic surfaces for flutter.
3. Verify pogo modes and measure damping.
4. Obtain transfer functions from the engine and control surfaces to the Guidance and Pointing System/Inertial Navigation System (GPS/INS) sensor locations for vehicle control.
5. Identify control surface nonlinearities for flutter.
6. Validate thermal protection system (TPS) dynamics.
7. Update the vehicle finite element model (FEM) using measured frequencies and mode shapes.
8. Use test-verified FEM to reassess flight loads, pogo, flutter, and flight control stability margins before first flight to insure safety.

In relation to these objectives and additional goals of characterizing/verifying the launch facility hardware and airbag isolation system, a total of 8 test configurations have been selected for the GVT. These include (a) two component tests for the avionics bay and INS substructure, (b) two vehicle mass simulator tests, in launch and GVT configurations, and (c) four X-33 vehicle tests (empty, partial fuel, full fuel, and TPS dynamics).

A number of objectives were also identified for pre-test analysis of the X-33 vehicle. These included determination of target modes (primary and secondary), accelerometer and shaker locations, impact of various mass simulators on vehicle system modes, and impact of the suspension system regarding coupling with vehicle modes. In addition, it was required to develop accurate

reduced Test Analysis Models (TAMs) for each vehicle configuration, and to conduct simulations to verify the adequacy of sensor and shaker locations.

For large complex and built-up structures such as X-33, a large number of sensors and shakers are typically used in order to validate the finite element model (FEM). The FEM with and without the thermal protection system (TPS) visible is shown in Fig. 3. Due to cost, installation or removal, and accessibility issues, only a limited number of sensors and shakers are generally available for placement. It is important that sensors and shakers be optimally placed in order to accurately measure the frequencies and mode shapes of the test article and validate the FEM. The validated FEM can be used for predicting vehicle loads, dynamic response, and the flutter margins.

Target Mode Selection

For target mode selection, four techniques were considered. These were (a) Root-Sum-Square (RSS) displacement method, (b) Modal Kinetic Energy approach, (c) Modal Cost approach, and (d) Balanced Singular Value approach. In general, these methods locate and rank modes having the highest participation or displacement when considering all degrees-of-freedom (DOF) or a subset of all DOF in the model. This approach is not fail-safe because some local modes have high energy but are still not target modes. Visual inspection is then required for the highest-energy modes to determine if they meet the criteria for target modes, i.e., that they be global vehicle modes, aerosurface modes, or modes of interest to pogo, for example.

The first step in selecting target modes was to determine the frequency ranges of interest for the different disciplines and requirements. Requirements were discussed in the previous section, in regard to objectives for the GVT. Table 1 lists the various requirements in the test objectives, along with the frequency ranges for primary and secondary modes. Frequency ranges were identified from inspection of modes predicted by the model (to determine the nature of the modes) and from consideration of the needs in each discipline or requirement area.

Most of the difficulty encountered in target mode selection was due to the nature of the X-33 structure and the finite element model. The model shown in Fig. 3 has about 120,000 DOF, and is characterized by a large number of localized, high-density modes. There are approximately 900 modes in the frequency band 0-55 Hz for each configuration, making visual inspection impossible except as a means of verifying analytical mode selection results. Many or most of these modes were local modes of the TPS and support structure, fuel tank surfaces, fuel lines, various lumped masses, and other items. Analytical approaches were required to sort through the hundreds of modes and identify potential modes of interest. The general approach taken was to use several such tools to drastically reduce the number of modes being considered, and then to verify through visual inspection which modes were indeed target modes.

Root-Sum-Square Displacement Method

A mode shape is defined by the ratio of the amplitudes of motion at the various points on the structure when excited at its natural frequency. If one of the elements of the eigenvector is assigned a certain value, the rest of the elements are also fixed because the ratio between any two elements is constant. The Root-Sum-Square (RSS) method (Hidalgo, 2000) takes advantage of this fact. Orthonormal modes are used in the RSS method. Normalization to a unit value of the largest eigenvector displacement is applied to the entire model (all the DOF) for all the modes.

Direct comparison between modes for a given vehicle fuel fill condition and for a particular location can be done, as well as comparison between modes from different fuel fill conditions (flight configurations) for a particular location. Modes of interest can be identified by visually noting the degree of modal displacement or deformation at a certain location on the structure. For example, noting the vehicle modes in which the canted fin actually distorts identifies canted fin modes. The RSS computes the magnitude of resultant modal displacement values for each mode at selected degrees of freedom (DOF) and sorts to locate modes with highest values. This is expressed in Eq. (1),

$$\{\text{RSS Resultant Value}\}_j = \sum [\phi^2_x+\phi^2_y+\phi^2_z]^{1/2} \qquad \text{Eq. (1)}$$

where $\{RSS\}_j$ is the summation magnitude value for mode j, and the ϕ's are the eigenvector translation coefficients for mode j for the selected nodes of interest.

The modes with the highest RSS displacement values have the highest overall motion and energy for that particular location or set of nodes. For the canted fin example, several hard points could be chosen along the span and chord and spaced such that expected mode shapes are reasonably covered. Then keying on the RSS displacement values of these nodes, and considering all fuel-level conditions, literally thousands of non-interesting modes are easily and effectively filtered out, leaving only modes of interest. It has been shown that four points can pick up the canted fin modes from the thousands of X-33 FEM vehicle modes. As for vehicle target modes, it has been shown that 86 nodes (out of 22,000 FEM nodes) can identify all the vehicle modes within a 0-25 Hz band. Above this range for the model, all target modes were control surface modes, which were determined individually.

Additionally, the RSS software sums the absolute modal displacement in the three axis directions for each mode,

$$R_{xj} = \sum|\phi_x|,\ R_{yj} = \sum|\phi_y|,\ R_{zj} = \sum|\phi_z| \qquad \text{(Eq. 2)}$$

where R_j is the absolute summation value for mode j in the x, y, and z component directions. Again, the RSS routine sorts to locate modes with highest values. This yields insight into the directional modal dynamic behavior of the modes. For example, longitudinal or pogo modes were identified in this fashion by looking at modes with the highest R_x summation values. In the canted fin example, the directional summation (R_x, R_y, and R_z) values would give insight as to which bending mode was being identified by resultant RSS displacement value.

In the next section, the modal kinetic energy approach is described, and RSS results will be shown in comparison to target modes identified by that technique. Both approaches allow a determination of modes having highest energy or overall displacement for all DOF in the model or a set of DOF, and it is instructive to look at the results together.

Modal Kinetic Energy (Generalized Mass) Approach

This straightforward method is based on calculations of generalized mass on a mode-by-mode basis, which provides a measure of the kinetic energy of all the DOF in the model for a given mode shape. However, the mode shapes must be normalized to maximum displacement to obtain meaningful information from the calculations. As shown in Eq. (3), the modal kinetic energy is given by the diagonals of the generalized mass,

$$[KE] = \text{diag}\,[\Phi^T \mathbf{M}\Phi] \qquad \text{Eq. (3)}$$

In this expression, Φ is the matrix of free-free modes (vehicle on suspension system), and **M** is the mass matrix. Comparison and ranking of these diagonal values provides a means of determining which modes have the most energy across all the DOF in the model, and are thus candidate target modes.

The modal kinetic energy (MKE) approach when compared to, and used with, the RSS method provides a very powerful approach for filtering out weak or localized modes and identifying potential target modes. These two approaches achieve similar results in that high-energy modes are located. However, the difference in the methods is that the MKE approach uses all the model DOF, while RSS is normally used with a strategic set of points ("control" points) covering all regions of interest on the structure. The implications of this are that MKE will often "flag" high-energy modes where many parts of the structure are moving, but the the modes are not of interest for model correlation. In contrast, the RSS approach allows the analyst to filter out such high-energy non-interesting modes by a proper choice of control points. The two methods taken together are extremely powerful and thorough, for several reasons:

1. The MKE approach rarely misses a potential target mode, but often finds non-interesting modes. However, the analysis must be careful in choosing the threshold value of kinetic energy.
2. The RSS approach does not flag non-interesting high-energy modes, and helps in determining if modes flagged by MKE are truly global modes (or modes involving regions of interest if localized).
3. The MKE approach provides insurance when using RSS, in the event that selected control points for RSS are missing an important region of the structure.

Results for the MKE and RSS methods are presented together for the reasons discussed here. When the top-ranked modes from both MKE and RSS are taken together, and then examined visually for verification, the analyst can have high confidence that the strongest modes of interest have been located. Table 2 shows typical results for the RSS method and MKE or generalized mass approach, both for the empty vehicle case. Double asterisks (**) indicate very strong modes relative to the minimum value threshold, and single asterisks (*) indicate modes that are weaker but should still be considered as candidate targets.

Balanced Singular Value Technique

Blellock and Carney (1993) provide an overview & description of two modal selection techniques, one based on approxiamte balanced singular values, and a second method based on the modal cost. Both of these modal selection techniques order the modes in terms of their contribution to the input/output dynamics of the model. In addition, both algorithms are based on the assumption of light damping and sufficiently separated modes, which was hardly the case for the X-33 model.

The approximate balanced singular value approach is based on Moore's internal balancing (1981) technique. Moore's internal balancing techniques states that the controllability and observability grammians can be transformed into a balanced system such that the balanced singular values would be equal and diagonal. The approximate balanced singular values for sufficiently separated frequencies and light damping for each mode is then given by:

$$\sigma_i^2 = \frac{\sqrt{\phi_i^T \phi_{i1} + \omega_i^2 \phi_{2i}^T \phi_{2i} + \omega_i^4 \phi_{3i}^T \phi_{3i}}\,\sqrt{\psi_i \psi_i^T}}{2\zeta_i \omega_i^2} \qquad \text{Eq. (4)}$$

where

σ_i = ith balanced singular value
ζ_I = ith modal damping ratio
ω_I= ith modal frequency (rad/sec)
ϕi=matrix of mode shape coefficients at output location i
Ψi=matrix of mode shape coefficient at input location i.

Modal Cost Technique

Skelton (1980) proposed the Modal Cost Technique as a target modal selection procedure. The weighting for each mode is based on the contribution of that mode to the output energy for an impulse input. The modal cost for each mode is defined as follows:

$$MC_i = \frac{\psi_i^T \psi_i [\phi_{1i}^T \phi_{1i} + \omega_i^2 \phi_{2i}^T \phi_{2i} + \omega_i^4 \phi_{3i}^T \phi_{3i}]}{4\zeta_i \omega_i^3}$$

Eq. (5)

Note that the modal cost (*MC*) and the approximate balanced singular values (σ_i) are closely related by the following relationship:

$$MC_i = 4\zeta_i \omega_i [\sigma_i^2]^2$$

Eq. (6)

Final Determination of Target Modes for the Three Vehicle Configurations

For final determination of target modes for each vehicle configuration, modes were ranked using the RSS, MKE, Modal Cost, and the Balanced Singular Value methods, then examined visually to determine which highly-ranked modes were truly the target modes of interest to fulfill the GVT objectives. Figure 4, for example, shows the Modal Cost and the Balanced Singular Value indices plotted against all the X-33 vehicle modes in the frequency range of 0-55.0 Hz.

The target mode selection approach described here worked very well. However, in some cases it was quite difficult to decide when a mode should be eliminated. Some modes had high kinetic energy, and were global in nature, but very highly coupled with localized motion. Such modes would be extremely difficult to correlate with test data. It was decided to not retain such modes as targets, but to carefully observe the test modes in the event that these eliminated FEM modes are important.

Table 3 shows the composite list of target modes (to about 17 Hz) for two vehicle fuel-level configurations. Many strong global modes and other modes of interest can be found in all three configurations, but some modes can also be seen that are unique for a given configuration. Figure 5 shows two important target modes for the vehicle empty configuration, which were determined using the procedures described in this section.

Sensor Placement Techniques

For large complex structures such as X-33, because of the weight and cost considerations, a limited number of sensors are available and must be placed on the structure in an optimum fashion. Minimization of weight and cost of instrumentation will severely limit the sensor resources available. Selecting the right set of sensor locations for modal testing is critical in obtaining a high degree of correlation between the test results and the analytical model. Determination of the proper number and location of sensors and shakers is therefore an essential part of any pre-test analysis process.

For the X-33 vehicle, a total of four sensor placement techniques were investigated. The sensor techniques investigated included three conventional methods, WAKE, **M**/**K** ratio, and engineering judgement methods. In addition, an optimum sensor placement algorithm was also used for determining accelerometer locations. These techniques, and results obtained using them, are described in this section and the corresponding subsections of the paper.

In recent years, several procedures for selecting sensor locations for the purpose of modal testing and correlation have been investigated. Papadopoulous and Garcia (1993) developed a comprehensive list of common sensor placement techniques. Some of the most common standard sensor placement techniques include the Kinetic Energy (KE) method and its variants, the Average Kinetic Energy (AKE), and the Weighted Average Kinetic Energy (WAKE) methods, the Guyan Reduction (GR) and its variant, the (**M**/**K**) method, and the Effective Independence (EI) method. All of these techniques produce suboptimal solutions at best. The Kinetic Energy and the Guyan Reduction methods are non-iterative methods, whereas the Effective Independence method is an iterative technique.

Parker *et al.* (1983, 1990) proposed the use of Kinetic Energy (KE) or Average Kinetic Energy (AKE) method for sensor placement. It is assumed that by placing the sensors at points of maximum kinetic energy, the sensors will have the maximum observability of the structural parameters of interest. Degrees of freedom with the maximum kinetic energy for a mode or modes of interest would be chosen as desired sensor locations. Because of the mass weighting associated with this approach, there is an inherent bias against the placement of sensors in the areas of the structure in which a fine mesh size, and thus small mass, is used. That is, it picks locations in coarser-meshed regions where the mass is larger.

Chung *et al.* (1993) proposed the Weighted Average Kinetic Energy (WAKE) as a better and more refined tool for placement of sensors. The purpose of using the WAKE method is to obtain a weighted average kinetic energy across a given set of target modes on a DOF-by-DOF basis. The candidate set of sensor locations correspond to those degrees of freedom with large kinetic energy averaged across the entire set of target modes.

The **M**/**K** ratio method of sensor placement is based on the so-called master DOF in Guyan reduction (Guyan, 1965, and Penny *at al.*, 1992). Simply stated, the DOF in the model having the highest diagonal **M**/**K** values are

selected as master DOF, or sensor locations. These DOF having high inertia in comparison to stiffness, when retained as masters or candidate sensor locations, are known to yield Guyan reduced models that usually represent the lowest-order modes quite well.

Reference to Figs. 1 and 3 will be helpful in regard to the following discussions and subsequent sections, for identifying the various structural components of the X-33 vehicle. The locations of the liquid oxygen (LOX) and liquid hydrogen (LH2) tanks, aerosurfaces (canted and vertical fins and body flaps), intertank structure, the thrust structure, aeroshell, and thermal protection system (TPS) and its supports can all be seen in Figs. 1 and 3.

Initially it was reasoned through engineering judgment that the vehicle "hard points" and load paths of the primary structure would make the best candidate sensor locations for measuring global vehicle modes. The X-33 primary structure includes the LOX and LH2 tanks, the intertank structure connecting the tanks, the thrust structure at the rear of the vehicle, and the aerosurfaces. Essentially, this includes most of the vehicle except the TPS and the support structure for TPS. Figure 6 shows the first attempt at a sensor set based solely on engineering judgment. The engine, main and nose landing gear, ballast ring (near nose of vehicle), and areas with relatively large mass concentration (such as batteries) were also selected for measurement points in this initial set. In the following subsections the analytical approaches investigated, and results obtained with the techniques, are discussed. It is noted that throughout the process, analytical techniques were combined with engineering judgment to maintain reasonableness and develop a sensor set that could be implemented in the GVT.

Weighted Average Kinetic Energy (WAKE)

The Weighted Average Kinetic Energy (WAKE) method was investigated first for the purpose of sensor placement. As seen in Eq. (7), the expression for kinetic energy on a DOF basis is quite simple,

$$KE = \Phi \otimes M\Phi \qquad \text{Eq. (7)}$$

where the symbol $\otimes$ indicates term-by-term multiplication, and the mode shape and mass matrices have been defined previously for Eq. (3). To obtain the weighted average values across all the target modes, the minimum and average values of kinetic energy for each DOF across all target modes are used:

$$WAKE = KE_{min} \otimes KE_{avg} \qquad \text{Eq. (8)}$$

A combination of NASTRAN DMAP alter and a FORTRAN sorting program was used to rank, sort and identify the candidate set of sensor locations.

Using this approach, it was found that the more flexible locations such as the aerosurfaces and outer skin of the vehicle were ranked highest. For analysis in which the top 10,000 DOF, or about 3300 points, were determined, the distribution of highest-ranked points was as follows: (1) aerosurfaces, 1586 points combined; (2) windward skin (aeroshell), 661 points; (3) LOX, 142 points; (4) engine mass simulator, 102 points; (5) thrust structure, 92 points; (6) LOX feedline, 92 points; (7) ballast, 88 points; and (8) avionics bay, 77 points. It is noted that the windward skin was highly ranked because it was modeled as lumped masses attached to the support structure, with the result that some of those DOF were very active. Figure 7 shows the distribution of WAKE points (based on top 3300 locations) for the cutaway view of the model without the outer skin (TPS).

The top 3300 points selected by the WAKE method were used in combination with engineering judgment to obtain a more reasonable number of points for further consideration. For example, the windward skin points were eliminated (since it was known that none or only a few points would be instrumented there), and a generous but much smaller set of aerosurface points was used. A set of about 1300 points was retained at this stage for further analysis. Guyan reduction was performed, retaining the translational DOF at these 1300 points as master DOF. For the empty or no-fuel case, Table 4 shows a comparison of Guyan-reduced model target-mode frequencies (to about 28 Hz) in comparison to the full model, along with the Modal Assurance Criteria (MAC) and cross-orthogonality values. In general, the Guyan model based on WAKE results was only accurate for the first few global modes of the vehicle and for "pure" aerosurface modes (clean aerosurface modes, not significantly coupled with other motion).

Diagonal Mass-to-Stiffness Ratio (M/K)

The next approach investigated was the mass/stiffness ratio method related to Guyan reduction. Degrees of freedom having the highest mass/stiffness ratio were determined by computing the diagonal **M**/**K** values for the model (using a NASTRAN DMAP alter) and then ranking them from largest to smallest within a separate algorithm.

For analysis in which the top 10,000 DOF (about 3300 points) were retained, as was done for the WAKE method, the distribution of highest-ranked points was as follows: (1) windward skin (aeroshell), 802 points; (2) LH2 tanks, 496 points each; (3) LOX, 263 points; (4) base, 182 points; (5) LH2 frames, 136 points; (6) thrust structure, 128 points; (7) aerosurfaces, 98 points combined, and (8) avionics bay, 96 points. As was noted for the WAKE results, the windward skin was highly ranked because it was modeled as lumped masses attached to the support structure. Thus, many DOF had relatively high inertia and low stiffness. Figure 8 shows the distribution of highest-ranked points for the mass/stiffness ratio method (model cutaway view without outer skin). Figure 8 is also based on the top 3300 points for comparison to WAKE results in Fig. 7.

The number of initially selected points (3300) was modified and reduced by engineering judgment to obtain a smaller and more reasonable set (same size as for WAKE)

for further evaluation. This was done by (1) eliminating the windward skin points for the reason described previously, (2) eliminating excessive numbers of points for several components, (3) removing points located inside the LOX and LH2 tanks that the method selected, and (4) providing a better distribution of points on the aerosurfaces. As was done for the WAKE method, a set of about 1300 points was retained for further consideration.

Guyan reduction was performed using the translational DOF at the 1300 points. For the empty vehicle case, Table 4 compares the reduced- and full-model (target mode) frequencies, and shows the MAC and cross-orthogonality values, up to 28 Hz. A pattern similar to that observed for the WAKE method is seen, in that the Guyan model based on maximum diag(**M**/**K**) results was fairly accurate only for the first few global modes of the vehicle and for very clean aerosurface modes. As seen in Table 4, accuracy for the first few target modes is about the same as for the WAKE method, but overall, the mass/stiffness ratio method did not perform as well as WAKE. This is due to the fact that the mass/stiffness ratio method works well typically only for the lowest order modes, while the WAKE method utilizes the set of target modes of interest to determine the most active points. For the X-33 vehicle, the target modes include not only several low-order modes, but also higher-order modes spread throughout the 0-55 Hz bandwidth.

Another pattern observed in Table 4 is that Guyan reduction appears to lack the accuracy for producing an acceptable test-analysis model (TAM). This perhaps should not be surprising, since Guyan reduction is typically used to obtain reduced models accurate for fundamental or lower-order modes. Accuracy of Guyan models is known to deteriorate for modes higher in the frequency bandwidth.

Engineering Judgment

Initially, an engineering judgment approach was used independent of the Weighted Average Kinetic Energy (WAKE) and mass/stiffness ratio results. Rather, the X-33 hardware design and the dynamic model were studied to gain insight into possible sensor locations. The following guidelines were used in this effort:

1. Critical load paths of the vehicle and "hard points" were utilized to enhance model verification for loads analysis, and to minimize localized mode effects in the measurements. These areas of the vehicle included the intertank region, thrust structure, LOX and LH2 stiffened regions, and the landing gear.
2. Critical areas for control and flutter were covered extensively: avionics and all aerosurfaces.
3. Initially, the LOX and LH2 frames (TPS support structures) were covered extensively on both the tank-side edges and TPS-side edges. In this manner, TPS (aeroshell) effects were accounted for without going directly to the TPS panels, which was found to introduce undesirable localized modes into the reduced model. (A moderate number of points were to be added later for characterizing TPS dynamics.)
4. All components thought to be of possible interest were covered extensively. These included the ballast, nose, batteries, and others.

The model was basically given good general coverage in the initial engineering judgment set. Vehicle coverage was similar to that shown in Fig. 6, but fewer points were used on the LH2 tanks. Locations on the four main longitudinal stiffeners (top, bottom, and sides) were selected for each LH2 tank (Figs. 1,3) to reduce the number of points in comparison to Fig. 6 but still capture the motion of interest seen in the target modes.

Approximately 1300 points were obtained by engineering judgment to allow a reasonable comparison with the WAKE and **M**/**K** ratio results. In Table 4, results are shown for the empty vehicle case to 28 Hz. As before, Guyan reduced model frequencies are compared to the full model, and MAC and cross-orthogonality values are listed. In comparison to the results for the WAKE and **M**/**K** ratio methods, respectively, the engineering judgment sensor set performed generally as well as either method. It performed about the same for the lowest order target modes, much better for the canted fin elevon modes (18.3-18.5 Hz range), and worse for some modes in between.

In a subsequent iteration, the points on the TPS support frames (both LOX and LH2) were removed to observe the effect. The resulting 773-point set showed considerable improvement in MAC and cross-orthogonality values for several modes. This result appears to be due to the presence of hinged fitting mechanisms in the LOX frames, which were designed to accommodate contraction of the tank. For reasons not fully understood, the Guyan reduced model was less accurate when points near the hinges were included.

Engineering Judgment Analysis Combined with WAKE and M/K Results

Subsequent efforts were focused on reducing and improving the engineering judgment set by incorporating results from the WAKE and **M**/**K** ratio methods, and also utilizing visual target mode shape inspection. The WAKE method was the primary help in this process. For example, the candidate measurement location set for the canted fins was reduced by plotting the highly-ranked WAKE results on a structure plot of the canted fin model, and using those results as a guide to determine which points in the engineering judgment set to keep or modify. In addition, the bending target modes were visually inspected to observe the locations of peaks or inflection points in the modes. The peaks were seen to match the WAKE rankings to a large degree; highly-ranked points were often on or near a peak in the bending modes.

Results from the WAKE method were also helpful in verifying the selection of LOX measurement points, and

both the **M**/**K** ratio and WAKE results were useful for LH2 points. In some cases, such as the LOX, it was clear that up to half of the 117 points in the first engineering judgment set could be removed. The critical load paths (stiffened regions of the LOX) were followed in choosing points to retain.

In relation to the thermal protection system (TPS) and its supports, something of a problem was encountered. Based on the design of the TPS support structure, with its hinges and joints for alleviating thermal expansion/contraction, it was expected that uncertainty would be introduced into the test results. Low shaker forces in modal testing possibly would not free the joints, or nonlinearities would result if some joints were freed and others remained stuck. From this point of view, it would be desirable to instrument areas near these joints in order to characterize nonlinearities due to joint friction. There was also a need to monitor the dynamics of the TPS in the GVT. Thus it was realized that the final sensor set should include some points on the TPS and supports. However, instrumenting the TPS panels would also introduce a large number of localized modes into the reduced model and the measurements, making it more difficult to identify the vehicle global modes. Partly for this reason, the TPS and support points were not included in the candidate set discussed in this section.

Following the process of combining engineering judgment with WAKE and **M**/**K** ratio results, a set of 443 points was determined. Figure 9 shows that this smaller set still defines the shape of the vehicle quite well. Table 5 presents a comparison between the Guyan-reduced model to the full model for the empty vehicle case. Overall, this set performed as well as the 773-point engineering judgment set (which was the original 1300-point set minus TPS support points). The results in Table 5 were considered the best results that had been obtained to that point in the analysis based on engineering judgment, WAKE, and **M**/**K** ratio results. For this reason, the 443-point set will be used as a reference for further discussions in this section. However, it is noted that this reference set needed to be reduced further because of the sensor count limit of approximately 400. Additional studies were conducted to reduce the sensor set to 338 points without significant loss in accuracy. This set was well within the limits on number of accelerometers established for the GVT.

Optimum Sensor Placement Technique Based on Genetic Algorithm (GA)

The fourth sensor placement technique which was considered was based on experimenting with a *S*ensor & *A*ctuator *P*lacement *O*ptimization (*SAPOPT*) algorithm which was developed by Bedrossian (1998). *SAPOPT* is based on a Genetic Algorithm (GA) search technique combined with an efficient sensor and placement metric based on Hankel singular values. *SAPOPT* was developed primarily for optimizing real-world large sensor and shaker placement problems. For X-33 for example, the maximum number of sensors which was allowed for placement was 400 triaxial accelerometers (1200 channels).

Genetic algorithms (GA) are efficient broadly applicable global stochastic search algorithms which are based on the theory of evolution. The basic principles of genetic algorithms (GA) were first laid down rigorously by John Holland, his colleagues, and his students at the University of Michigan (1975). Holland's pioneering work showed that the GAs can be applied to solve a wide variety of problems. Genetic algorithms have been successfully applied to problems in biology, computer science, engineering, operations research, image processing and other areas. They are well suited for sensor and shaker placement optimization problems which are defined as integer combinatorial optimization problems.

The placement algorithm for sensors and shaker placement is based on a performance measure of observability for sensors, and controllability for shakers, as an indication of how well the system can be observed or controlled with a given set of sensors and/or shakers. For joint consideration of sensor and shaker placement problems, a metric based on the Hankel singular values of the controllability & observability grammians is formulated and is combined with the hybrid GA search technique for optimal sensor and shaker placement.

For the X-33 optimum sensor placement experiment, the *SAPOPT* algorithm was used in order to initially place 200 triaxial sensors on the vehicle in an optimum fashion. The sensor placement options which are implemented within *SAPOPT* include a) MAC-based criterion, b) determinant of Fisher Information Matrix (FIM) Based criterion, and c) Hankel Singular Value (HSV) based criterion. Initial tests were conducted by attempting to place 200 sensors in an optimum fashion using the MAC criterion. Even though sensor placement experiments using *SAPOPT* produced excellent MAC results based on the optimum sensor set with off diagonal terms below 0.05, the proposed optimum 200-sensor sets produced poor cross-orthogonality results. Other experiments included sensor placements based on determinant of FIM based criterion, and Hankel Singular Value (HSV) based criterion. Figure 10 and 11 show plots of the GA optimization using FIM and HSV criteria for sensor placement. The HSV-based sensor placement technique is believed to be the best criterion and was therefore used for X-33 sensor placement experiments as well.

Final Determination of Sensor Set

As can be seen from the analyses described in this paper, determination of the final sensor set was an iterative process. The genetic algorithm search method provided excellent MAC matrices (based on model partitioning, not model reduction), but the cross-orthogonality values for the Guyan-reduced vs. full models were not accurate enough. (Note again that Guyan reduction was used as the measure of comparison for various sensor sets.) In comparison, the combined engineering judgment,

WAKE/**M**/**K** ratio method produced reasonably accurate orthogonality values for most target modes, as well as fairly accurate MAC values and frequencies in most instances.

The final set of accelerometer locations was a combination of the genetic algorithm optimization results and the engineering judgment/WAKE/**M**/**K** results. This was done by further reducing the best "combined technique" 338-point set discussed in a previous subsection and merging it with the genetic algorithm results. Redundancies between the two sets were eliminated, yielding a set of approximately 400 points. This set was referred to as the "final round 1" set. A "final round 2" (and last) set was obtained from round 1 by providing a redistribution of some points selected by the genetic algorithm and the other methods to provide more symmetry and better coverage of the vehicle components. Figure 12 shows the locations of some of the points in the final 401-point set, as well as the distribution (number) of points on each vehicle component.

A number of parameter studies were done relative to the final set, because the Guyan-reduced models were not sufficiently accurate, as was the case for the reference 443-point set. Table 6 shows representative results of these parameter studies for the empty vehicle case. Results in Table 6 revealed that the "round 2" or last set (genetic algorithm points redistributed more symmetrically compared to "round 1") was somewhat better than "round 1".

Determination of Shaker Locations

The final portion of the X-33 pre-test analysis to be described is the determination of adequate shaker locations for the ground vibration test (GVT). Four different approaches were investigated in this effort. As noted previously, the number of shakers for the test was limited to approximately 6, such that analysis was merited to determine the best locations on the structure and thus save valuable time at the test site.

Weighted Average Drive Point Residue

Parker *et al.* (1990) proposed the Driving Point Residue (DPR) as a technique for selecting the best locations and directions for exciting a structure. DPRs are stated as being equivalent to modal participation factors, and are a measure of how well each mode is excited, or participated in the overall response. DPRs are also proportional to the magnitudes of the resonance peaks in a driving point Frequency Response Function (FRF) measurement. The point and direction of excitation are chosen where the DPRs are maximized (to excite a given mode), or minimized (to avoid exciting a given mode). the Weighted Average Driving Point Residue (WADPR) for shaker placement.

Equation (9) gives the definition of the drive point residue,

$$[\mathrm{DPR}] = [\Phi] \otimes [\Phi\ ]\ \{\Omega\} \qquad \text{Eq. (9)}$$

where Φ and Ω are the target modes and frequencies squared, respectively, and the symbol $\otimes$ indicates term-by-term multiplication. The weighted average DPR (WADPR) is defined as

$$[\mathrm{WADPR}] = [\mathrm{DPR}]_{\min} \otimes [\mathrm{DPR}]_{avg} \qquad \text{Eq. (10)}$$

This technique was developed to locate points on the structure that respond most (are most active) across the entire set of target modes. It has been used with considerable success and is available in commercial software packages for pre-test analysis.

Figure 16 shows the highest-ranked WADPR points for the vehicle in the empty configuration. It can be seen that the technique overwhelmingly selected points on the outer parts of aerosurfaces: canted fins and elevons, body flaps, vertical fins and rudders. Obviously, these locations are very active in the target modes. Several points were also selected on the avionics bay and LOX area TPS supports, but none of the points selected were considered attractive for exciting the global target modes of the vehicle.

Locations considered best (engineering judgment and accessibility considerations) for exciting the global target modes were the vehicle "hard points" and load paths, including the thrust structure, forward and aft jacking points, and hoisting points. None of these locations were ranked highly by the WADPR method. In the top 2000 DOF ranked by the method, none of the locations considered most desirable appeared. For the top 20,000 DOF, several desirable hard points were included, but they typically were not ranked highly.

The unsatisfactory results obtained with WADPR led to consideration of other approaches, including a genetic algorithm search technique, engineering judgment (already mentioned in this section), and a frequency response approach combined with engineering judgment.

Engineering Judgment and Frequency Response Analysis

The shaker drive locations described in the WADPR section as being desirable for exciting global target modes from an engineering judgment point of view and accessibility considerations are listed below:

1. Thrust structure, hold-down posts (support vehicle on the launch pad)
2. Forward and aft jacking points
3. Forward hoisting points

The forward jacking point is adjacent to (just aft of) the nose landing gear, and the aft jacking points are on the bottom (windward side) of the thrust structure hold-down posts (Fig. 2). The forward hoisting points are located to

the outsides of the LOX tank, near the nose landing gear station.

These points, along with many other points on the vehicle for comparison, were evaluated using a frequency response approach. This analysis involved a simulation of shaker (or impact hammer) inputs at the DOF selected for evaluation. Frequency response functions (acceleration/force, simulating test data) were computed at the excitation point and at a number of "control" points located literally all over the vehicle. The purpose of this analysis was to determine if the entire vehicle responded to excitation at the candidate shaker points. Computer code was developed to search the response function maxima to locate target mode resonant peaks. The basic concept in this approach is that if most or all target frequencies can be located in the drive-point response or other control point responses for a given excitation DOF, the excitation point is a good shaker location. Comparison of responses for the various candidate shaker locations allows selection of the best excitation points.

Analysis was done for the empty vehicle case to 25 Hz using the approach described here. Peak searching of the response functions was utilized to find the best excitation location for each direction, and the candidate shaker points were ranked separately for the X,Y, and Z drive directions. The best locations for each direction are listed below, in ranked order:

X-direction
1. Thrust structure, top center
2. Aft jacking, -Y side
3. Forward hoist, -Y side
4. Thrust structure, top right corner (+Y)
5. Thrust structure hold-down, +Y

Y-direction
1. Forward hoist, +Y
2. Forward hoist, -Y
3. Aft jacking, +Y side
4. Thrust structure hold-down, -Y
5. Thrust structure, top right corner (+Y)

Z-direction
1. Forward jacking
2. Thrust structure, top right corner (+Y)
3. Thrust structure, top center
4. Engine, -Y side
5. Aft jacking, +Y side
6. Forward hoist, -Y side

To demonstrate how drive-point response functions compare for good excitation points vs. poor ones, Fig. 14 shows Y-direction drive-point responses for a forward hoisting point (excellent shaker location) and a vertical fin (poor location for global vehicle modes). In the case of the hoisting point, many peaks can be observed, which is a good indication that many target modes are being excited. For the vertical fin, the flexibility of the fin dominates the response, and the other peaks are barely visible. Thus it is difficult to excite Y-direction global target modes with an excitation point on the vertical fin. On the other hand, the fin response function shows how effective driving on the fin would be if the objective was to characterize its dynamics in isolation from the vehicle dynamics.

GA Optimum Shaker Placement Technique

SAPOPT sensor and actuator placement algorithm was once again used for placing an optimum set of shakers on the vehicle for the purpose of modal parameter estimation. Due to constraints associated with access to the interior of the vehicle during GVT and other related issues, an initial shaker set based on engineering judgment was first created, and SAPOPT was then used to minimize that set to 6 locations as shown in Fig. 15.

Final Determination of Shaker Locations

As was the case for target mode and sensor location selections, the final set of shaker locations was also a combined product of several techniques. The WADPR results verified how active the aerosurfaces are across the set of target modes, and that very active response would occur for drive points on the canted fins and vertical fins. However, a technique utilizing a search of response function peaks showed that global vehicle (bending and torsion) modes would not be well-excited for aerosurface shaker locations, but that driving at the vehicle hard points provided excellent energy distribution in the vehicle.

A final set of shaker locations was the product of all the analysis and engineering judgment including the GA-based optimization techniques. Figure 15 shows the locations on the vehicle for different excitation directions. This set should provide adequate excitation of all global vehicle modes and excitation for verification of aerosurface modes (of interest for flutter and controls).

To evaluate the effectiveness of the sensor and shaker locations for exciting the target modes, extensive numerical simulations were performed. Two well known simulation techniques were used. The first sensor and shaker location validation technique used is known as the Multivariate Mode Indicator Function (MMIF) (Williams, et.al, 1985). The valleys in the MMIF plots correspond to the roots in the system. Based on the plot in Fig. 16, the MMIF plot clearly shows that validity of the selected sensor and shaker set, since all target modes of the structure are clearly identifiable.

The second validation technique used is known as the Complex Mode Indicator Function (CMIF) (Shih, et.al, 1988). CMIF plots are generated by performing Singular Value Decomposition (SVD) of the Frequency Response Functions (FRFs) at each spectral line. The CMIF is a simple and efficient method for identifying the modes of a complex system. The CMIF identifies modes by identifying the magnitude of each mode. Since multiple reference data is applied in CMIF, repeated roots can be detected. Unlike the MMIF, which indicates the existence of real normal modes, CMIF indicates the existence of real normal or complex modes and the relative magnitude

of each mode. Based on the plot in Fig. 17, the CMIF also clearly shows that validity of the selected sensor and shaker set. In addition, the CMIF method not only identifies all target modes, but also identifies the magnitude of each mode.

Test Analysis Model (TAM) Reduction

There are five commonly used model reduction methods, Guyan (1965) or static reduction, Improved Reduced System (IRS) reduction (O'Callahan, 1989), modal reduction (Kammer, 1987), hybrid reduction (Kammer, 1991), and SEREP reduction (O'Callahan, 1991). Results discussed thus far for Guyan-reduced models of the X-33 vehicle have not shown the accuracy expected in comparison to full models for the target modes of interest. Normally, it is desired that the reduced model have target mode frequency errors within about 2 percent, and that the cross-orthogonality diagonal values be approximately 0.95 or greater, with off-diagonals 0.05 or less. Such accuracy of the reduced model is needed to provide the best opportunity for successfully correlating the model to test data. At this point, it was realized that advanced model reduction techniques could be required for achieving an accurate test analysis model (TAM). Actually, this is not surprising for the X-33 model, because the target modes are not all lower-order modes, but are typically scattered through the 0-55 Hz target mode bandwidth.

To assess the improvement achievable with the IRS model reduction technique, the reference 443-point candidate sensor set was used for the empty vehicle configuration. In Table 5, the IRS-reduced model frequencies are compared to the full model, and as before for Guyan reduction, the MAC and cross-orthogonality values are shown. Comparison of IRS results to Guyan reduction for the same DOF set shows (a) significant improvement for target modes up to 17 Hz, (b) accuracy similar to Guyan reduction for the four target modes from 17.8-18.6 Hz, and (c) somewhat worse performance than Guyan reduction for the target modes from 26.9-27.5 Hz. This discussion applies mainly to mode shape comparison; i.e., MAC and cross-orthogonality values. Frequencies obtained with IRS reduction were consistently better through the target bandwidth.

In summary for IRS reduction, it appears that significant improvement in accuracy for both frequencies and modes can be achieved for the lower-order target modes in comparison to Guyan reduction. However, the improvement achieved is still not sufficient to meet the standards for TAM accuracy described previously in this section.

These findings led to consideration of the hybrid reduction method. The hybrid approach allows development of a reduced model that is exact for the target modes and frequencies, because the target mode shapes are used in the transformation matrix for the method. In addition, the hybrid technique yields better results for non-target modes than does the modal reduction method, which is also exact for the target modes. Hybrid reduction was used for all three vehicle fuel-level configurations to develop highly accurate TAMs for the final sensor set described in Fig. 12. In all three cases, reduced-model target frequencies were exact, the diagonal cross-orthogonality values were 1.00, and the off-diagonal values were on the order of 1.0E-6. Figures 18 and 19 show orthogonality plots for the Guyan-reduced and hybrid reduced models, respectively, for the empty vehicle case. Comparison of the two figures shows the vastly improved model reduction accuracy achieved with the hybrid approach.

It was decided to use hybrid model reduction for the final sensor set to achieve the required accuracy for the TAMs. *However, Guyan reduction was still be used as the criteria for comparing the accuracy of various candidate sensor sets.* Hybrid reduction obviously cannot serve as such a comparative criteria because of its characteristics described in the previous paragraph. A possible objection to using hybrid or modal reduction is that a sparse sensor set could yield a very poor static reduction, but obviously also yield an exact hybrid/modal TAM. The implication is that one does not really know the quality of the candidate sensor set. This potential objection is circumvented in this investigation by doing comparative Guyan reductions for all candidate sensor sets to assess their robustness.

Summary

Pre-test analysis for the X-33 ground vibration test (GVT) has been described in detail for three configurations: empty, partially-fueled, and fully-fueled. The analytical approaches for determining target modes, sensor locations, and shaker locations were discussed. Although these methods are very powerful and useful, the role of engineering judgment was pivotal for maintaining reasonableness in the results. Knowledge of the vehicle and the model was indispensable in the test planning and analysis.

A major conclusion was that Guyan (static) reduction was insufficient for development of accurate test analysis models (TAMs). This was due to the target modes being scattered through the target bandwidth, rather than being predominantly lower-order modes. Further, performance of Guyan reduction was degraded by the presence of hinged joints in the LOX TPS support structure, and by the high flexibility of the LOX feedline. It was found that the hybrid reduction technique was required for acceptable accuracy in the TAMs.

Without exception, the target modes, sensor locations, and shaker locations were the products of combined analytical approaches and engineering judgment. No technique when used alone was found to be sufficient for any phase of the pre-test analysis. This is due to the complexity of the X-33 structure and model, with its joint mechanisms and highly flexible aeroshell, and the highly-coupled nature of the mode shapes.

References

Bedrossian, Herand (1998). *Optimum Placement of Sensors and Actuators For Modal Identification*, Ph.D. thesis, University of Southern California, Los Angeles, CA.

Blelloch, P.A., and Carney, K.S. (1993). *Modal Selection in Structural Dynamics*, Proceedings of the 11th International Modal Analysis Conference, Kissimee, Florida.

Chung, Y.T (1996). *Model Reduction and Model Correlation Using MSC/NASTRAN*, MSC/NASTRAN User's Conference, Los Angeles, CA.

Guyan, R.J. (1965). *Reduction of Stiffness and Mass Matrices*, AIAA Journal, Vol. 3, pp. 380.

Hidalgo, H. (2000). *An Innovative Structural Mode Selection Methodology: Application for the X33 Launch Vehicle FEM*, Paper to be presented at the AIAA Dynamics Specialist Conference, Atlanta, GA.

Holland, J.H. (1975). *Adaptation in Natural and Artificial Systems*, Ann Arbor,MI.

Kammer, D.C. (1991). *A Hybrid Approach to Test-Analysis Model Development or Large Space Structures*, Journal of Vibration and Acoustics, Vol. 113, pp. 325-332.

Kammer, D.C. (1987). *Test Analysis Model Development Using an Exact Model Reduction*, Int. J. of Analytical and Experimental Modal Analysis, Vol. 2, pp. 174-179.

Kammer, D.C. (1991). *Sensor Placement for On_Orbit Modal Identification and Correlation of Large Space Structures*, Journal of Guidance, Control, and Dynamics, V14, No. 2, pp. 251-259.

Kammer, D.C., and Triller, M.J. (1992). *Efficient Sensor Placement for On-Orbit Modal Identification of Sequentially Assembled Large Space Structures*, Proceedings of the 10th International Modal Analysis Conference, San Diego, Ca., pp. 954-964.

Moore, B.C. (1981). *Principal Component Analysis in Linear Systems, Controllability, Observability and Modal Reduction*, IEEE Trans. Autom. Control, vol. 26.

O'Callahan J., (1989). *A Procedure for an Improved Reduced System (IRS) Model*, Proceeding of the 7th IMAC, Las Vegas, NV, pp 17-21.

O'Callahan J., (1991). *A System Equivalent Reduction/Expansion Process (SEREP)*, Proceeding of the 7th IMAC, Las Vegas, NV, pp 17-21.

Papadopoulous, M. and Garcia, E. (1998). *Sensor Placement Methodologies for Dynamic Testing*, AIAA Journal, Vol. 36, No. 2.

Parker, G., Brown, J. (1983). *An Application of the Kinetic Energy Calculation as an aid in Mode Identification*, The Shock and Vibration Bulletin.

Parker, G., Rose, T., Brown, J. (1990). *The Kinetic Energy Calculation as an aid to Instrumentation Location in Modal Testing*, MSC World Users Conference, Los Angeles, CA.

Penny, J.E.T., Friswell, M.I., and Garvey, S.D. (1992). *The Automatic Choice of Measurement Locations for Dynamic Testing*, Proceeding of the 10th IMAC, San Diego, CA, pp 30-36.

Shih, C.Y., Tsuei, Y.G., Allemang, R.J., and Brown, D.L., (1988). *Complex Mode Indicator Function and Application to Spatial Domain Parameter Estimation*, Mechanical Systems and Signal Processing, Volume 2, Number 4, 1988.

Skelton, R. E., P.C. Hughes, (1980). *Modal Cost Analysis for Linear Matrix Second Order Systems*, Journal of Dynamic Systems, Measurement, and Control, Vol. 102, pp. 151-158.

Williams, R. Crowley, J. and Vold, H. (1985). *The Multivariate Mode Indicator Function In Modal Analysis*, 3rd IMAC,1985.

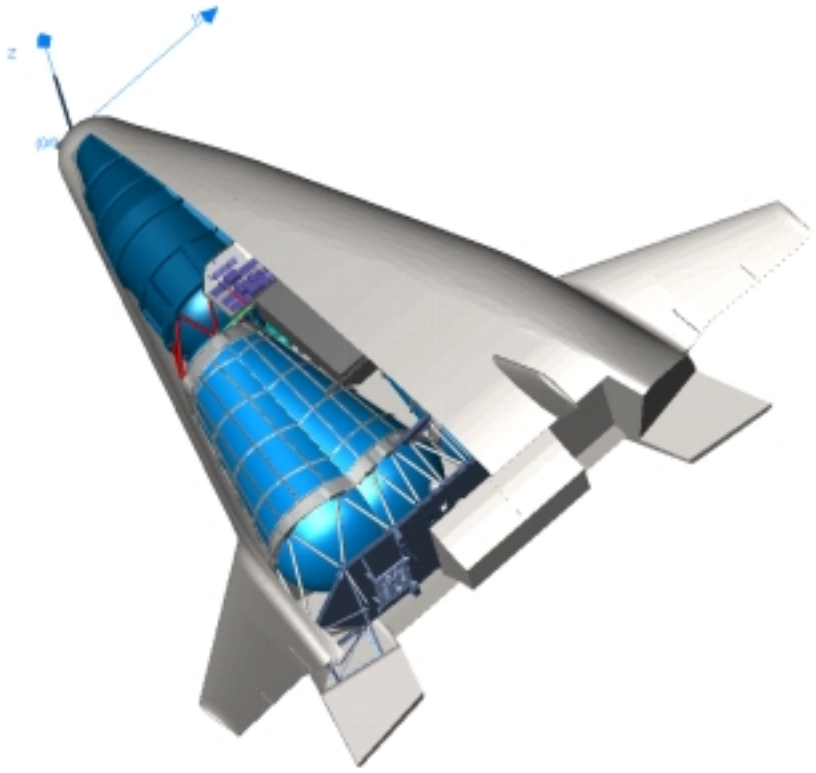

Figure 1: X-33 Vehicle

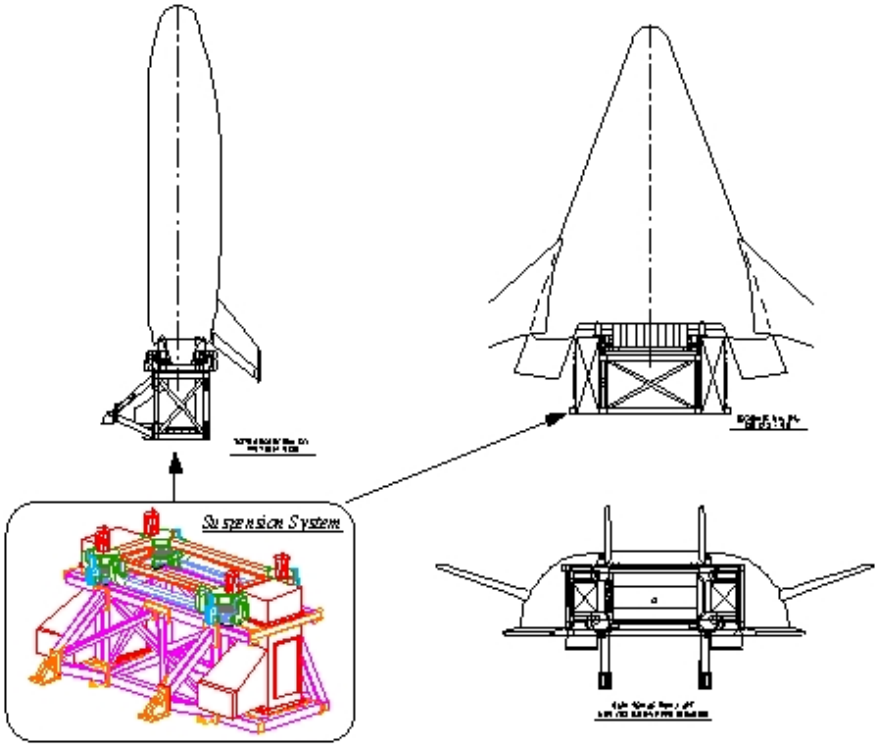

Figure 2: X-33 Vehicle on Suspension System for GVT

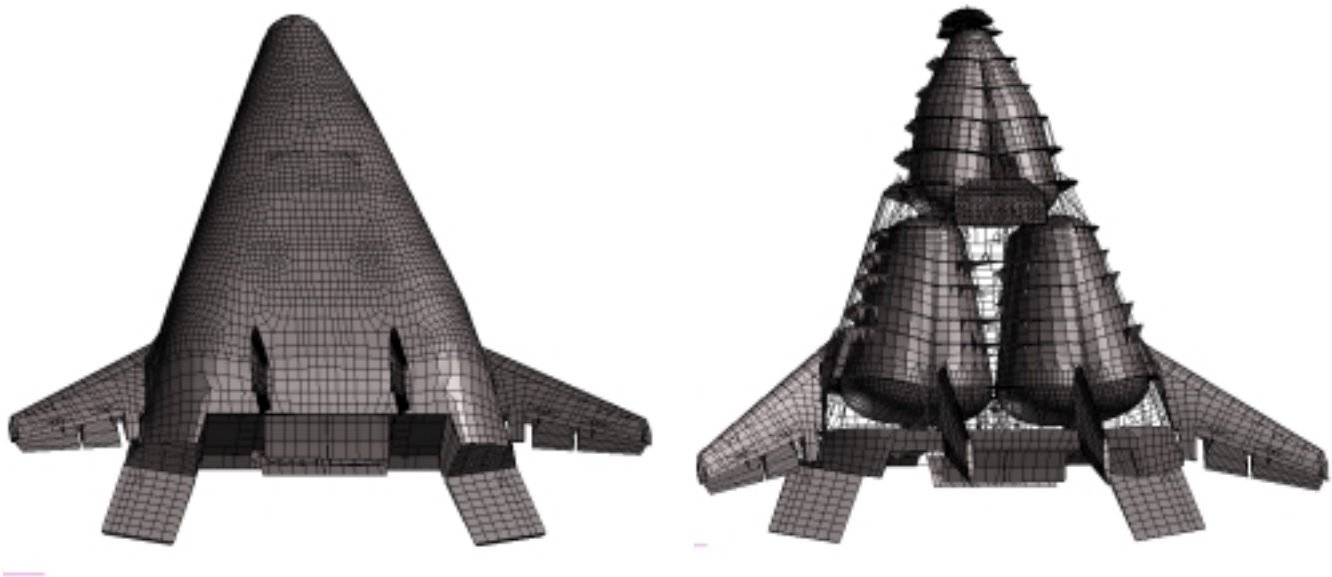

FEM with TPS **FEM Cutaway View**

Figure 3: X-33 Vehicle Finite Element Model (FEM) Representation

Table 1: X-33 Test Objectives and Frequency Ranges of Interest for Target Modes

TEST OBJECTIVE	Primary Modes	Secondary Modes
Vehicle Control	0 -15 Hz.	15 - 25 Hz.
Flutter & Aeroelasticity	0 - 55 Hz.	-
POGO	0 - 25 Hz.	25 - 35 Hz.
Aeroshell Dynamics	0 -100 Hz.	100-300 Hz.
Liftoff Transient Loads	0 - 25 Hz.	25 - 55 Hz.
Vehicle Dynamics	0 - 25 Hz.	25 - 55 Hz.

Table 2: Comparison of Results for RSS and Generalized Mass (Modal Kinetic Energy) Techniques

Mode #	Modal KE	FREQ. (HZ)		Visual ID	Modal RSS	FREQ. (HZ)		Description of Mode Shape
7	-	-			1.4	4.89		Nose Gear: (Canted fin Anti-Sym Very Weak)
8	2.6	4.95	*	(1)	4.5	4.95	* *	Canted Fin (Cf) Symetric
9	3.0	5.49	*	(2)	6.9	5.49	* *	Cf Anti-Sym: Veh delta torsion
10	1.7	5.73			2.1	5.73		Nose Gear (Ng): Cf Anti-Sym
11	14.0	6.49	* *		-	-		Localized Mode: LOX Web
14	5.0	7.74	* *	(3)	5.3	7.74	* *	1st Veh Z (Pitch) Bending: OP Ballast Ring
17	4.9	8.51	* *		1.2	8.51		Ballast Ring: LH tank Web
27	1.8	9.88		(4)	4.0	9.88	* *	1st Veh Y (Yaw) Bending
28	4.2	10.08	* *	(5)	2.5	10.08	*	Weak Veh Z Bending OP w/ Ballast
29	1.6	11.01			-	-		Localized LOX Tank/TPS
30	4.9	11.36	* *	(6)	7.2	11.36	* *	Veh "Jumping Jack" Anti-Sym (POGO)
31	5.0	11.56	* *	(7)	5.5	11.56	* *	Veh "Jumping Jack" Sym (POGO)
32	-	-			1.6	11.64		Localized LOX Tank/TPS
33	2.9	11.83	*		1.2	11.83		Body Flap (Bf): Ng/Ballast: Cf
34	1.5	11.89			2.3	11.89	*	Avionics Bay: Veh Z: Bf
35	1.8	11.99			2.9	11.99	*	Avionics Bay: Veh Z: Bf Phase Difference

Table 3: X-33 Composite List of Target Modes for Two Vehicle Configurations (P--Primary Modes, S--Secondary)

	FULL		EMPTY		
	Class-mode #	Freq. Hz	Class-mode #	Freq. Hz	Description
1	S-1	**0.18**	S-1	**0.30**	**Vehicle/suspension pitch mode about base**
2	S-2	**0.36**	S-2	**0.57**	**Vehicle/suspension yaw mode about base**
3	S-6	**1.49**	S-3	**1.28**	**Vehicle/suspension roll mode**
4	S-4	**1.37**	S-4	**1.62**	**Vehicle/suspension axial mode**
5	S-8	**2.25**	S-5	**1.73**	**Vehicle/suspension lateral (yaw about lox tank)**
6	S-9	**2.37**	S-6	**1.94**	**Vehicle/suspension normal (pitch about lox)**
7	P-13	**5.53 A**	-	**-**	**Vehicle/LOX Tank Torsion Mode // Partial + canted fin anti-sym**
8	P-15	**6.40**	P-7	**6.41**	**Canted fin symmetric bending**
9	P-16	**6.46**	P-9	**6.91**	**Canted fin anti-symmetric bending**
10	P-18	***7.77 B***	-	**-**	**LOX tank Z Bending/ Vehicle Z Bending**
11	P-19	**7.84**	-	**-**	**LOX Tank Y Bending + Vehicle Twisting about Base**
12	-	**-**	P-10	**8.32 A**	**Vehicle Torsion + Lox Frame 6&7**
13	-	**-**	-	**-**	**LOX Tank Z Bending: Vehicle Z Bending**
14	P-23	**8.85 C**	-	**-**	**LOX Tank Y Bending Mode**
15	-		-	**-**	**LOX Tank Y + Frame Lox 6&7**
16	S-24	***9.26 E***	-	**-**	**LOX Tank Twisting + Frames 6&7 +Canted Fin +Body Flap**
17	-	**-**	-	**-**	**LOX Tank Yaw w/ some Twist + Vehicle Twisting about Base**
18	P-32	**10.59**	P-18	**10.44**	**Body flap symmetric**
19	P-35	**11.05**	P-17	**10.20**	**Body flap anti-symmetric**
20	-	**-**	P-21	***10.90 B***	**Vehicle Normal (Z) Bending +Avionics Bay + Body Flap**
21	-	**-**	P-22	***11.00 C***	**Vehicle yaw (LOX tank)**
22	-	**-**	S-27	***11.42***	**Vehicle yaw**
23	P-40	**11.33**	-	**-**	**Canted fin in-plane : anti-symmetric**
24	-	**-**	P-28	***11.88 E***	**Vehicle yaw + frame 6&7 + Canted fin**
25	-	**-**	S-29	**11.99**	**Canted fin in-plane : symmetric**
26	P-42	**11.61**	-	**-**	**Vehicle Pogo mode and canted fin inplane symmetric bending**
27	P-45	**12.29 F**	-	**-**	**Vehicle Pogo model / Axial Mode (Cf in Plane w/ Vehicle)**
28	P-82	**15.49**	P-52	**14.14**	**Vehicle Z Bending**
29	-	**-**	-	**-**	**Pogo Axial Vehicle mode**
30	P-92	**16.74**	P-74	**16.75**	**Vertical fin anti-symmetric**
31	P-94	**16.92**	P-77	**16.97**	**Vertical fin symmetric**
32	P-97	**17.20**	-	**-**	**LOX Tank Bulge Mode (w/ LOX frame axial motion)**

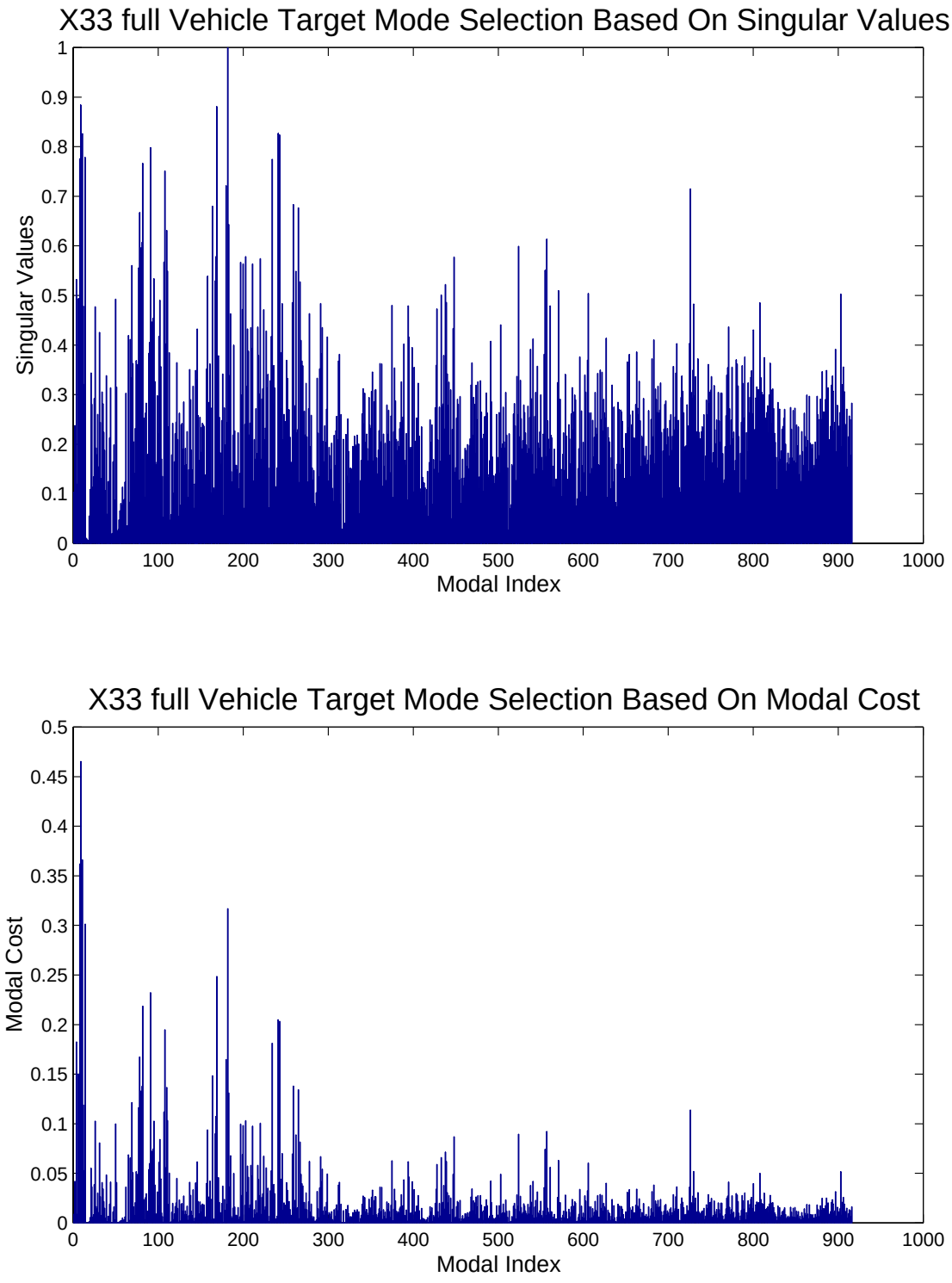

Figure 4: X-33 Vehicle Target Mode Indices (Upper Curve - Singular Value Index, Lower Curve- Modal Cost Index)

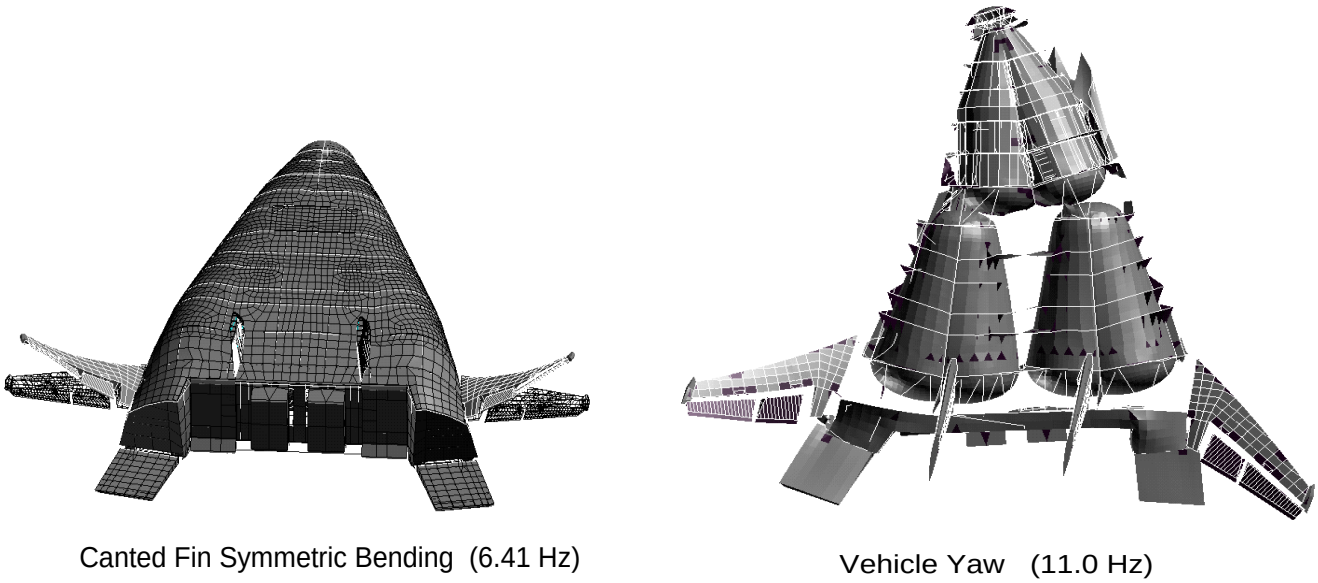

Figure 5: Examples of X-33 Vehicle Target Modes

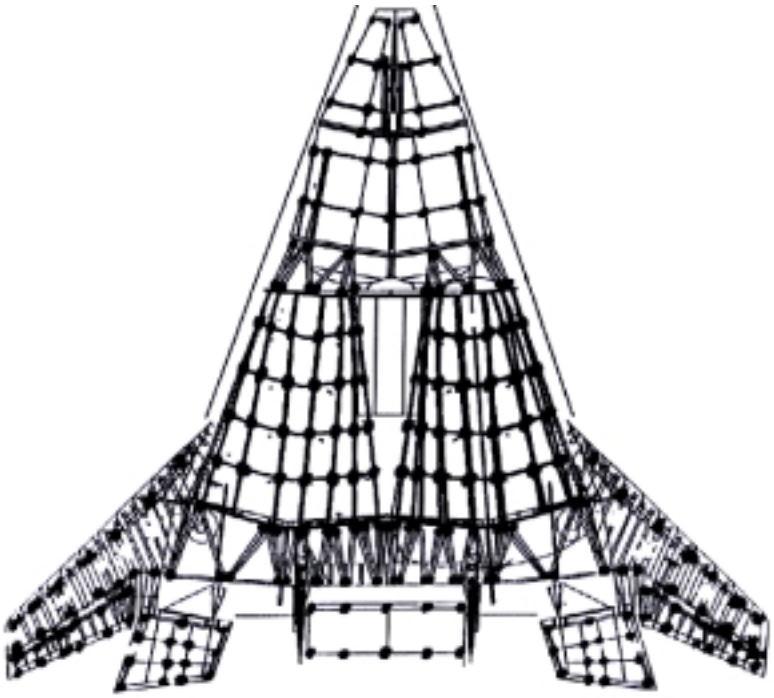

Figure 6: Initial Candidate Sensor Set Based on Engineering Judgment

Figure 7: Distribution of Sensor Points for WAKE Method (Based on 3300 Locations, Empty Vehicle, TPS not shown)

Table 4. Comparison of Guyan-Reduced and Full Models for WAKE, **M**/**K**, and Engineering Judgment Approaches (1300 Points, Empty Vehicle)

Full freq.	WAKE			M/K			Engineering Judgment		
	ASET freq.	MAC	XORT	ASET freq.	MAC	XORT	ASET freq.	MAC	XORT
6.41	6.43	.9973	.9572	6.43	.9999	.9961	6.42	.9999	.9965
6.91	6.94	.9992	.9602	6.94	.9998	.9607	6.91	.9997	.9653
8.32	8.45	.9993	.9900	8.50	.9984	.9934	8.47	.9991	.9939
10.20	10.12	.9289	.7974	10.26	.9957	.8808	10.32	.9950	.9033
10.44	10.45	.4125	.7211	10.46	.5029	.7712	10.58	.9665	.8407
10.91	10.78	.7809	.7309	11.10	.8551	.7489	11.08	.7518	.8346
11.00	11.09	.9361	.9594	11.34	.7803	.7381	11.14	.7273	.8008
11.42	11.52	.8492	.9290	11.34	.7766	.8138	11.84	.5955	.7784
11.88	12.44	.7410	.7526	12.54	.7043	.7722	12.69	.8267	.7047
11.99	12.00	.4499	.7598	12.08	.7129	.8179	12.07	.5125	.8257
14.14	14.32	.5777	.6789	14.60	.4623	.4099	14.68	.7449	.7409
16.75	16.75	.9944	.9781	16.85	.9901	.9627	16.86	.4870	.5342
16.97	16.99	.8831	.8474	17.01	.7926	.7127	17.10	.8258	.8376
17.84	17.80	.8480	.8735	18.26	.4064	.6626	17.92	.7826	.8632
18.35	18.34	.6535	.6976	18.93	.5050	.7428	18.40	.9657	.9572
18.54	18.55	.5087	.7219	18.72	.3205	.6175	18.58	.9868	.9601
18.58	18.64	.7937	.8920	18.93	.3973	.5723	18.65	.9484	.9725
26.88	26.84	.1477	.4288	27.07	.2149	.4056	27.05	.2442	.3523
26.98	27.14	.3535	.3942	27.31	.4137	.5565	27.24	.3018	.4320
27.33	27.47	.6559	.5702	28.24	.1904	.2467	27.49	.3332	.3095
27.45	27.59	.8970	.8110	28.39	.4688	.6478	27.61	.8473	.8504

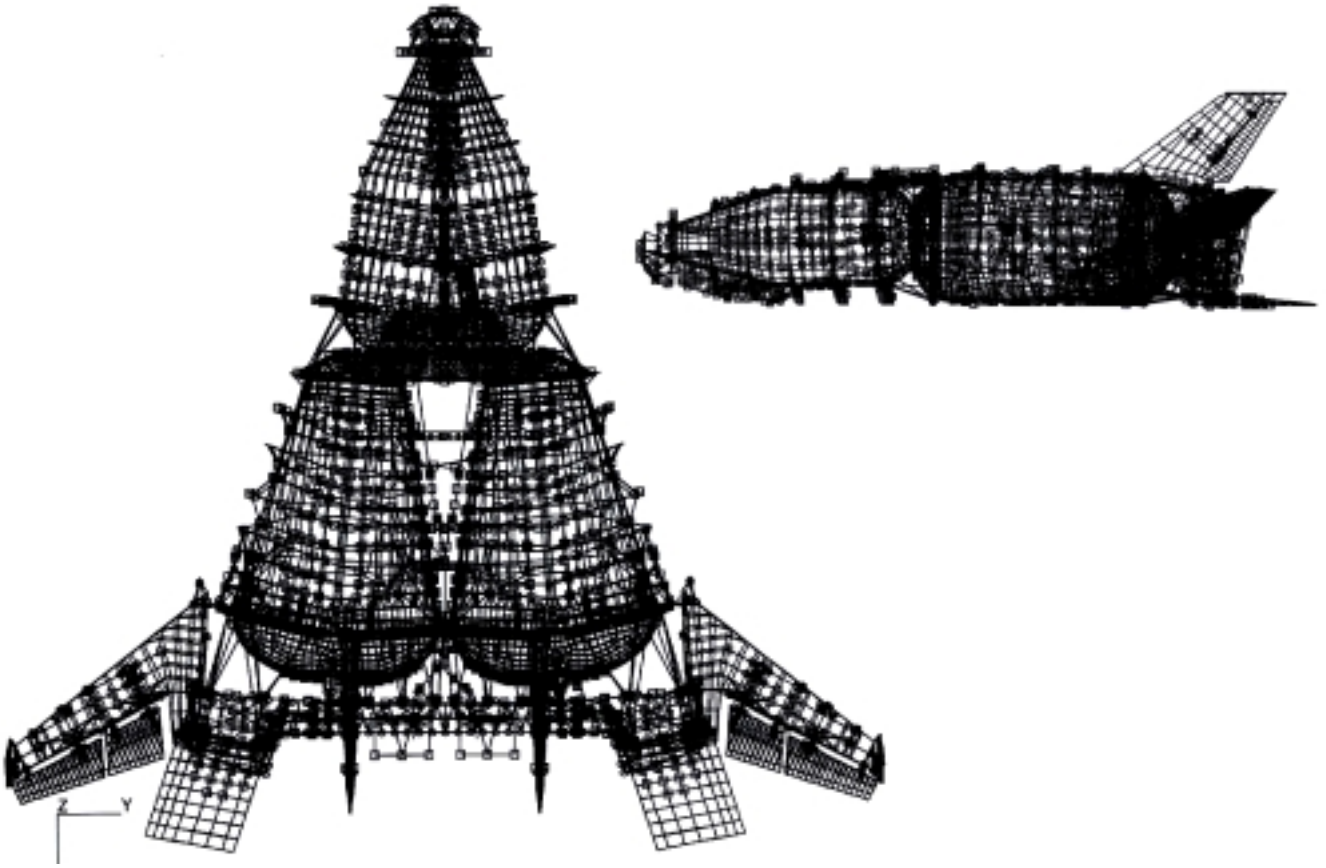

Figure 8: Distribution of Sensor Points for **M**/**K** Method (Based on 3300 Locations, Empty Vehicle, TPS not shown)

Figure 9: X-33 Vehicle Sensor Points for Combined Engineering Judgement, **M**/**K**, and WAKE (443 Sensor Locations)

Table 5. Comparison of Guyan-Reduced, IRS-Reduced, and Full Models for Combined Engineering Judgment, WAKE, and **M**/**K** Approaches (443 Points, Empty Vehicle)

Full freq.	Guyan Reduced			IRS Reduced		
	ASET freq.	MAC	XORT	ASET freq.	MAC	XORT
6.41	6.42	.9999	.9999	6.41	.9999	.9996
6.91	6.96	.9996	.9995	6.91	.9999	.9984
8.32	6.96	.5704	.5644	8.46	.9932	.9386
10.20	10.19	.9820	.9862	10.23	.9970	.9612
10.44	10.57	.9582	.9736	10.47	.9921	.9266
10.91	11.18	.8762	.9265	10.98	.9501	.7214
11.00	11.26	.8985	.9052	11.09	.9868	.9378
11.42	11.26	.7643	.8016	11.51	.8785	.8847
11.88	12.32	.8691	.9351	12.06	.8073	.7444
11.99	12.08	.9490	.9740	12.01	.8569	.8969
14.14	14.62	.7085	.8043	14.15	.9861	.8937
16.75	16.77	.9991	.9967	16.76	.9985	.9816
16.97	17.11	.9369	.7921	17.08	.9942	.7509
17.84	18.14	.8884	.9037	17.87	.7964	.7420
18.35	18.64	.7444	.8970	18.35	.9771	.8926
18.54	18.69	.9829	.9850	18.54	.9786	.9673
18.58	18.77	.8522	.8895	18.58	.9499	.8990
26.88	27.08	.7758	.7608	27.03	.7647	.3550
26.98	27.08	.7066	.5766	27.03	.6723	.4413
27.33	27.64	.6577	.6112	27.40	.7547	.4170
27.45	27.72	.9593	.9186	27.47	.9667	.7375

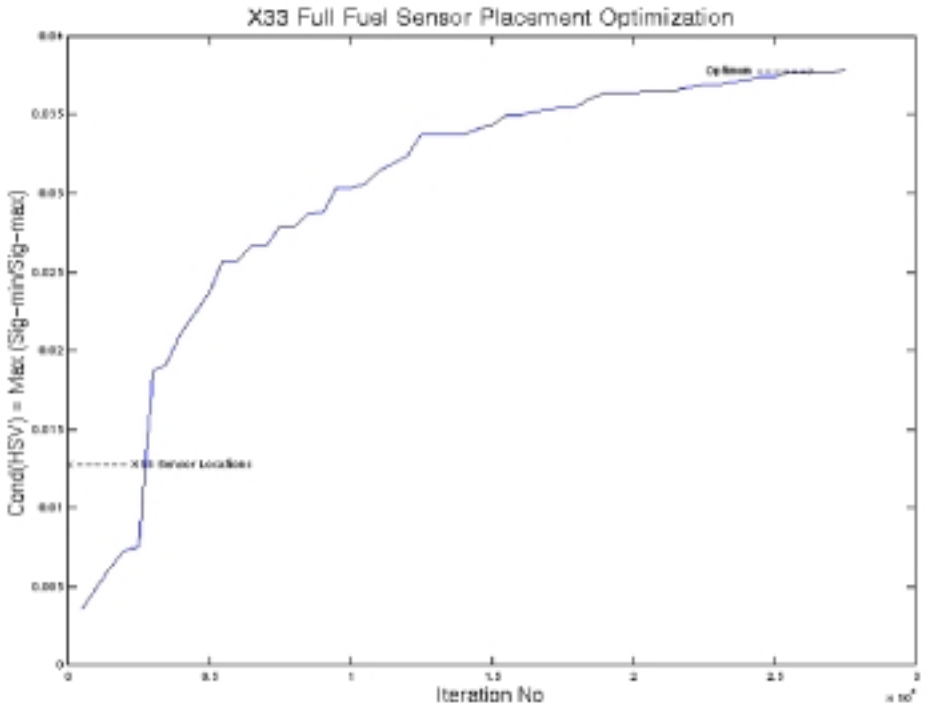

Figure 10: X-33 Sensor Placement Optimization Convergence History
Based on Condition Number of Hankel Singular Values (HSV)

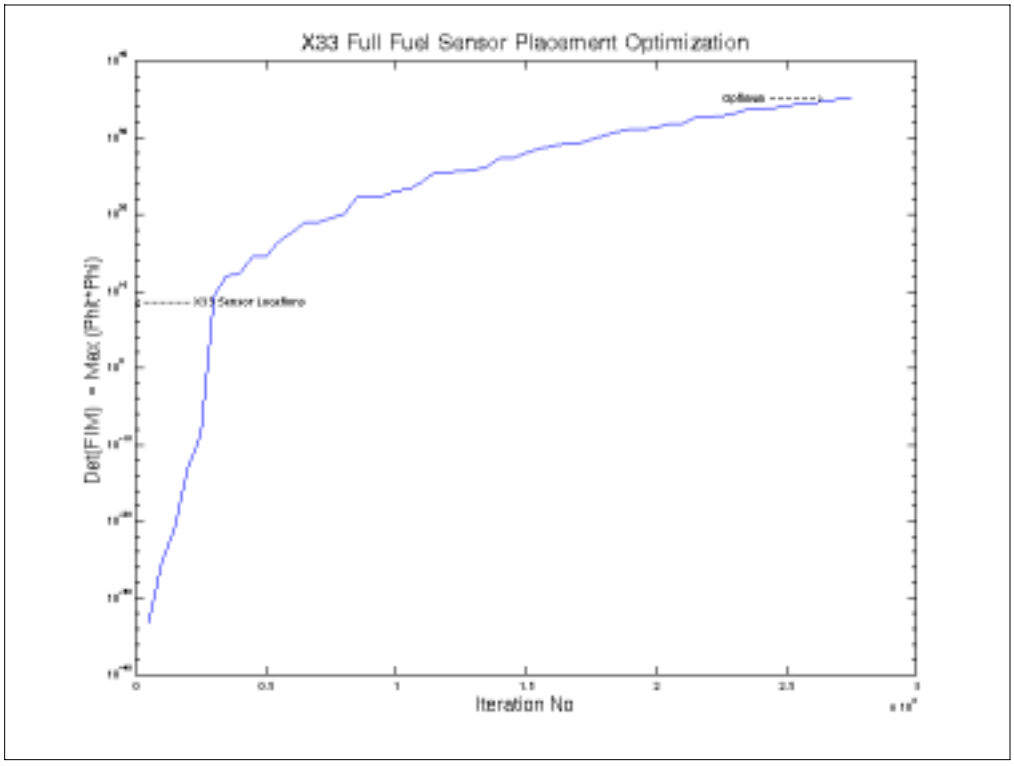

Figure 11: X-33 Sensor Placement Optimization Convergence History
Based on Determinant of Fisher Information Matrix (FIM)

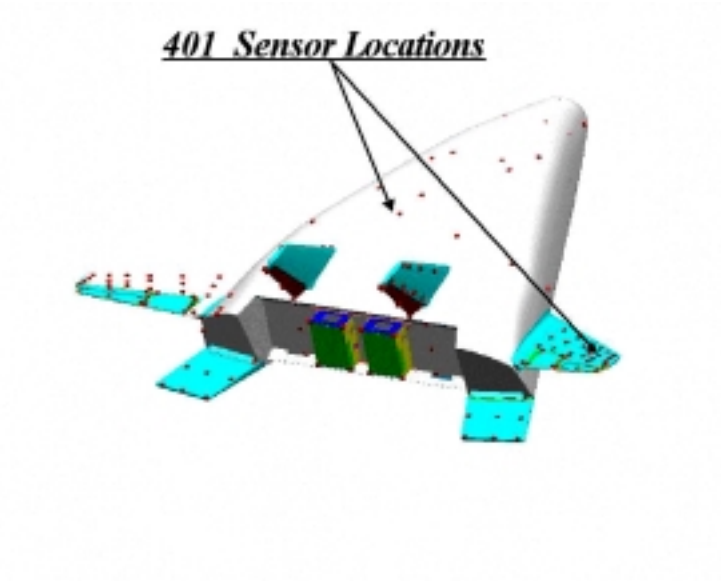

Location on Vehicle	No. of Accels
Seismic	6
Ballast ring	3
Main Landing Gear	8
Nose Landing Gear	7
LOX Tank	52
LOX Frames	13
INS/Mona Beams	13
Avionics Bay	15
LH2 Tank	57
LH2 Tank Beams	20
LH2 Frames	21
TPS Supports	25
Intertank	4
Body Flaps (2)	16
Canted Fins (2)	54
Vertical Fins (2)	32
Base	6
Thrust Structure	22
Engine	10
LOX Feedline	9
Suspension	8
Total	**401**

Figure 12: Final X-33 Vehicle Sensor Locations for GVT

Table 6: Comparison of Final Sensor Sets: Round 1 with Combined Engineering Judgment/WAKE/M/K and Original GA Results, Round 2 with Redistribution of GA Points for Improved Symmetry (** Indicates Round 2 Results Significantly Better than Round 1, * Round 2 Significantly Worse than Round 1)

Full freq.	Guyan freq. Round 2	Guy. freq. Round 1	MAC Round 2	MAC Round 1	XORT Round 2	XORT Round 1
6.41	6.42	6.42	.9999	.9999	1.0000	1.0000
6.91	6.93	6.94	.9999	.9987	.9999	.9994
8.32	**8.50	8.75	**.9914	.6325	**.9959	.8526
10.20	**10.31	10.38	**.9965	.8227	**.9969	.9221
10.44	10.48	10.48	**.5448	.4368	**.8082	.7612
10.91	11.16	11.14	*.5140	.6800	*.6423	.7650
11.00	11.48	11.46	.5621	.5458	.6706	.6581
11.42	**11.48	11.98	*.3563	.5768	*.5165	.7471
11.88	**12.58	12.65	**.6336	.4156	**.8025	.6382
11.99	12.07	12.08	**.6874	.5686	**.8935	.8587
14.14	14.97	14.98	.4979	.3423	.7803	.7657
16.75	16.79	16.79	.9920	.9869	.9953	.9871
16.97	17.12	17.12	*.8828	.9438	*.9136	.9413
17.84	17.96	17.96	.9371	.9424	.9110	.9094
18.35	*18.48	18.41	*.7361	.8030	**.7576	.6379
18.54	18.67	18.67	.9906	.9915	.9898	.9897
18.58	18.75	18.76	.9678	.9837	.9657	.9696
26.88	*27.10	26.82	**.5638	.4500	**.6203	.4066
26.98	*27.10	26.82	*.4791	.5372	**.7026	.4174
27.33	27.55	27.58	**.4904	.1377	**.5510	.4057
27.45	27.76	27.72	** .7694	.1321	**.7687	.5227

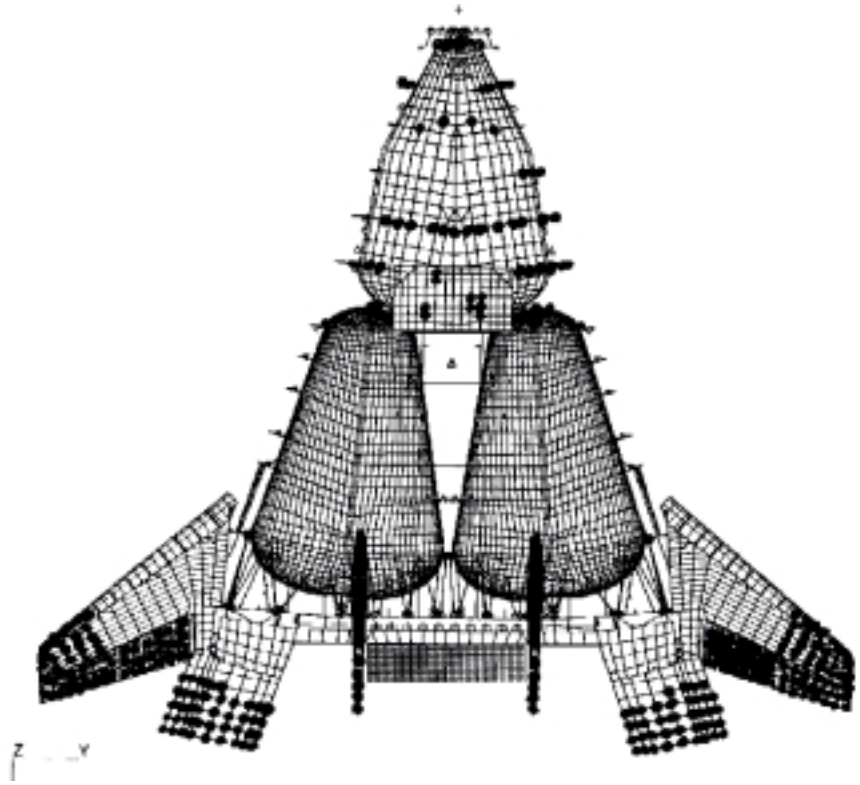

Figure 13: X-33 Vehicle Possible Shaker locations Based on WADPR

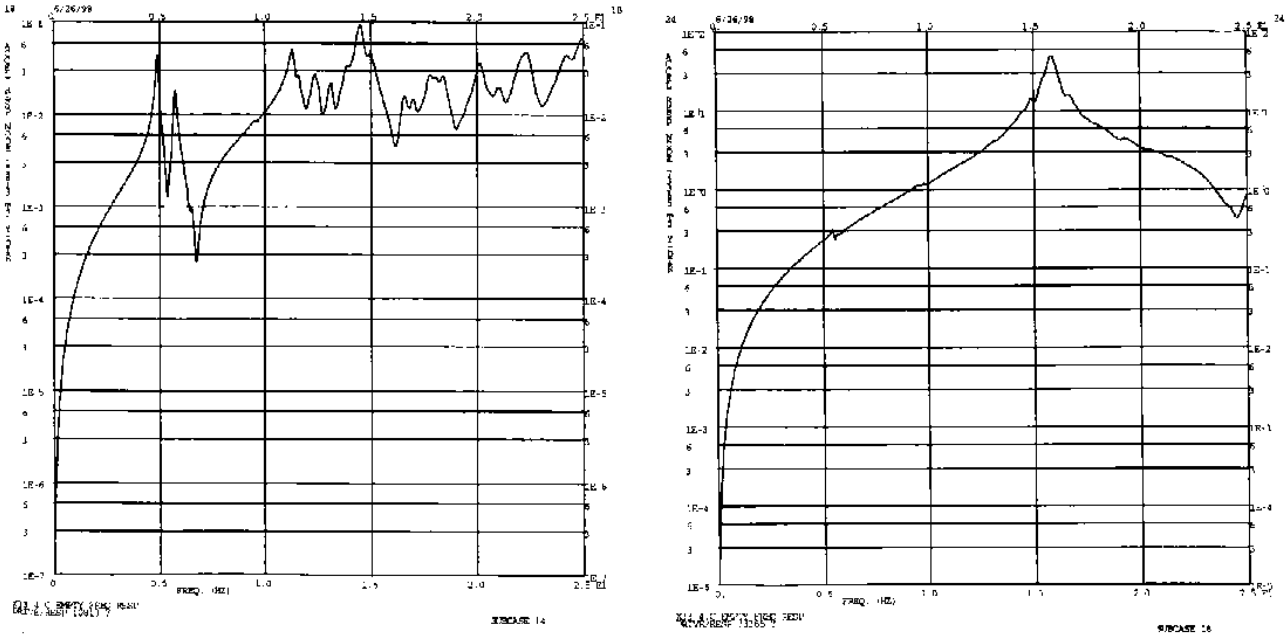

Figure 14: Comparison of Drive Point Response Functions for Good (Left) and Poor (Right) Shaker Locations for Exciting Global Target Modes

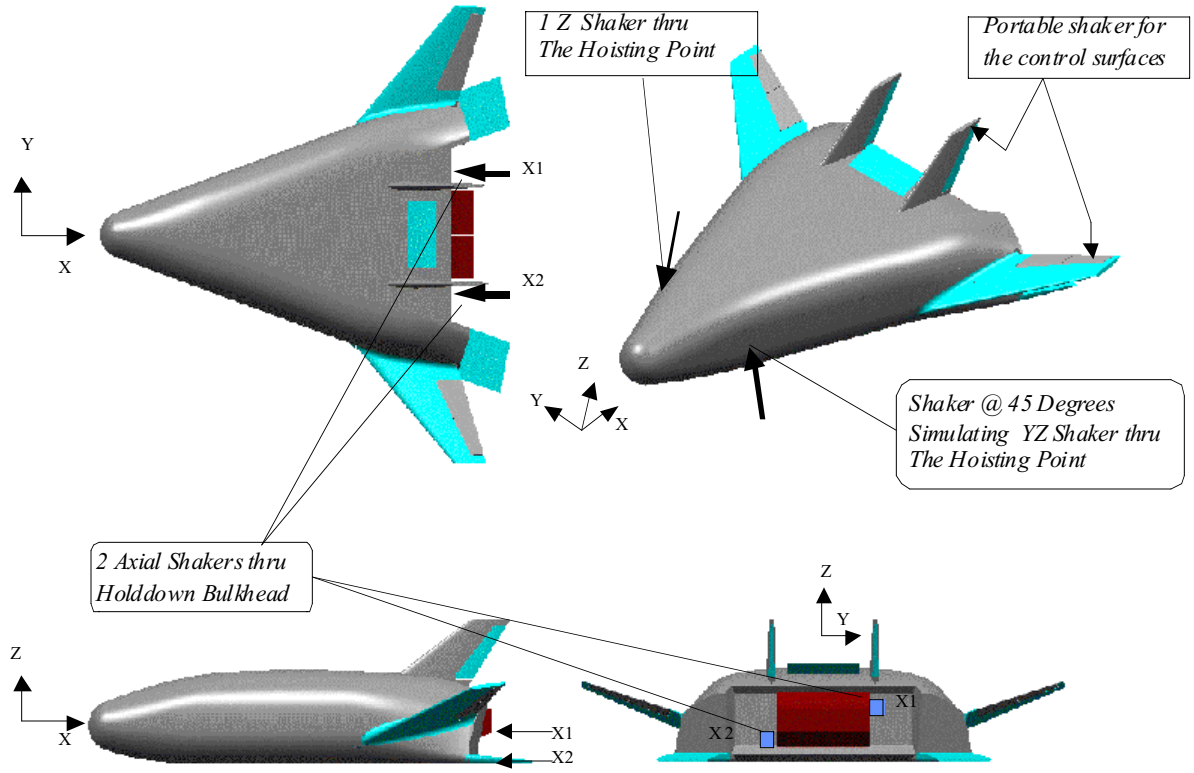

Figure 15: X-33 Vehicle Shaker Locations for GVT

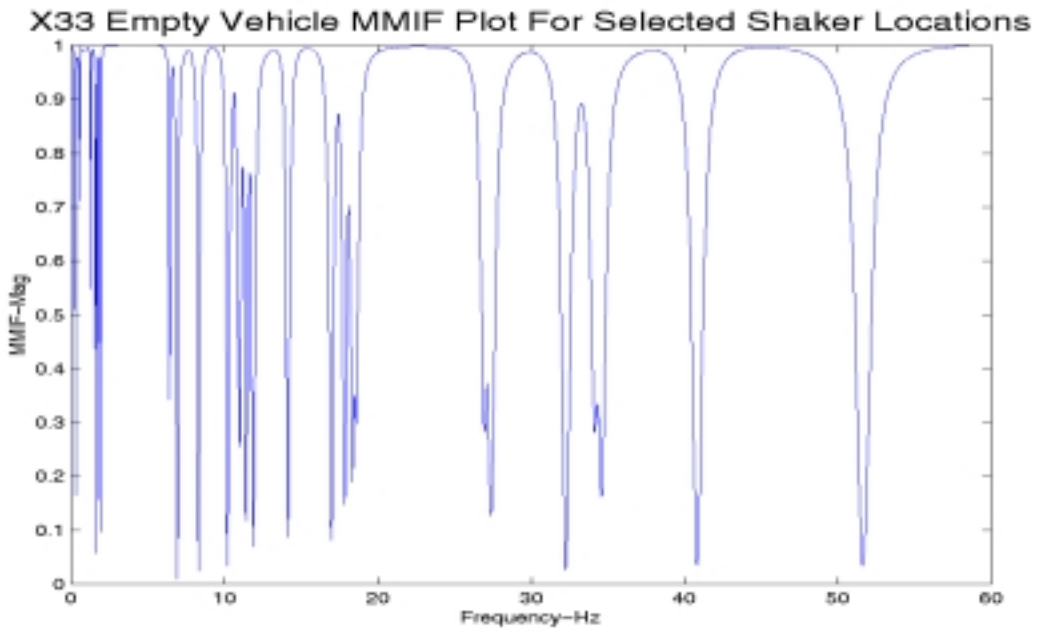

Figure 16: X-33 Sensor & Shaker Evaluation Based on Multivariate Mode IndicatorFunction (MMIF) Calculations Based on 401 Sensor & 5 Shaker Locations

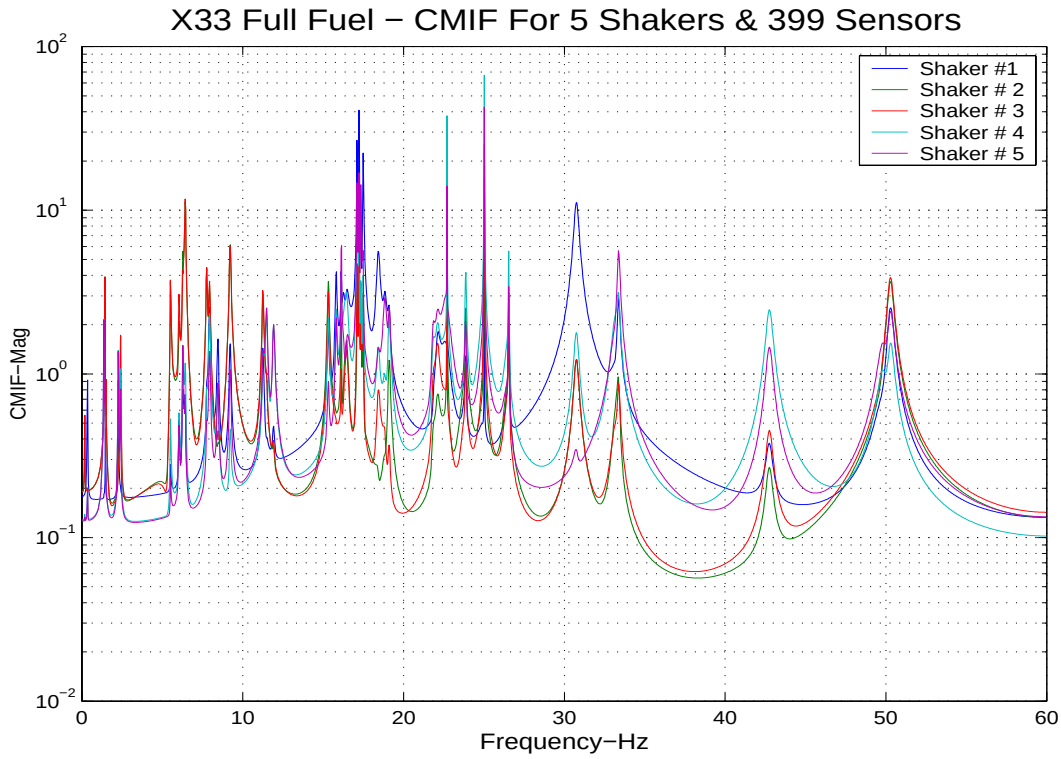

Figure 17: X-33 Sensor & Shaker Evaluation Based on Complex Mode Indicator Function (CMIF) Calculations Based on 401 Sensor & 5 Shaker Locations

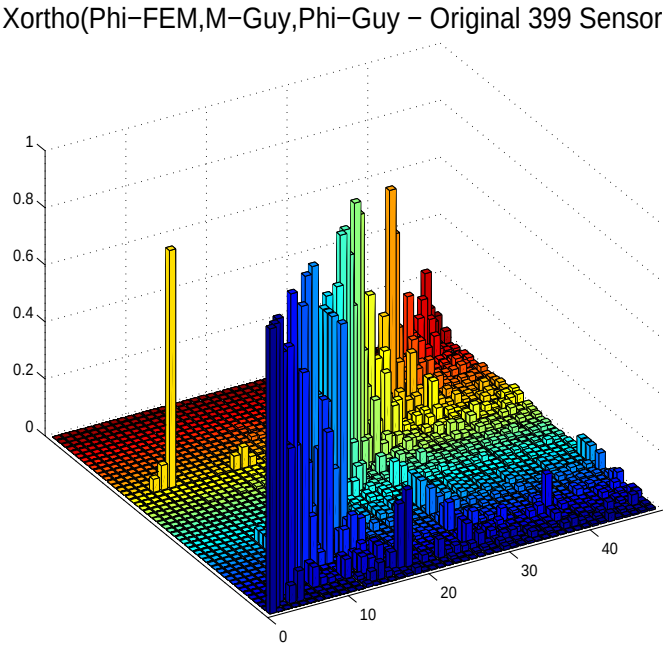

Figure 18: X-33 Cross-Orthogonality Plot Based on Guyan Reduction Technique

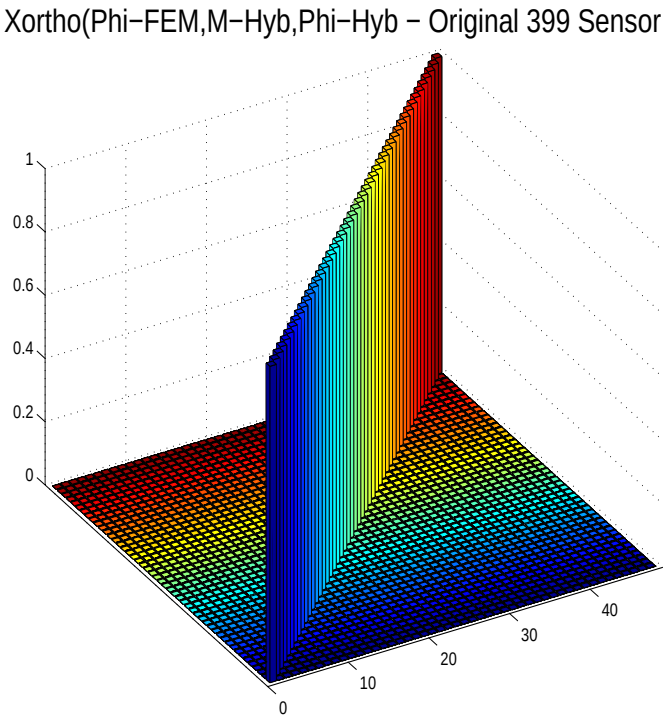

Figure 19: X-33 Cross-Orthogonality Plot Based on Hybrid Reduction Technique